Journal of Physics: Conference Series

PAPER • **OPEN ACCESS**

Airborne wind energy systems flying optimal trajectories in turbulent wind using flight path tracking

To cite this article: J-B Crismer *et al* 2024 *J. Phys.: Conf. Ser.* **2767** 072021

Airborne wind energy systems flying optimal trajectories in turbulent wind using flight path tracking

J-B Crismer[1], T Haas[2], M Duponcheel[1] and G Winckelmans[1]

[1] Institute of Mechanics, Materials and Civil Engineering (iMMC), Université catholique de Louvain (UCLouvain), 1348 Louvain-la-Neuve, Belgium

[2] Department of Electromechanical, Systems and Metal Engineering, Ghent University, 9000 Ghent, Belgium

E-mail: `jean-baptiste.crismer@uclouvain.be`

Abstract. Airborne Wind Energy Systems (AWES) consist of tethered wings harvesting power from the wind. Rigid-wing (aircraft) pumping-mode AWES are considered here: they generate power during the reel-out phase and consume a fraction of this power during the reel-in phase. Those devices fly complex trajectories that require advanced control strategies. In the present work, we aim to develop a Large Eddy Simulation (LES) framework and improve the fidelity of existing models. The toolbox `AWEbox` is used for reference trajectories generation and control. Here the device is operated with a closed-loop control using a 6-DOF aircraft model. The aircraft is modeled using an actuator line (AL) for the wing, and the effects of the control surface are incorporated using their geometry and lift slope. The AL-based model is used to assess the robustness of the nonlinear model predictive controller against turbulence and to compare the performance between idealized conditions in `AWEbox` and turbulent wind conditions in the LES. The controller demonstrates high efficiency in tracking the reference trajectory and extracting the maximum power, even at high turbulence levels.

1. Introduction

The concept of Airborne Wind Energy (AWE) emerged in the 70s and was first developed by Loyd [1]. The subject has received a renewed interest in the last decade due to its potential to produce green energy. The technology has several advantages over wind turbines, such as the lower material and infrastructure requirements, leading to a reduced carbon footprint [2], in alignment with the climate objectives. The technology is based on flying wings/kites and it comes in various concepts [3]. This study focuses on fixed-wing (aircraft type) pumping-mode airborne wind energy system (AWES). It is one of the most studied concepts, which operates in two phases. In the first phase, the reel-out, the kite flies a crosswind trajectory while pulling on a tether. The tether unwinds from a drum, located on the ground, driving a generator. In the second phase, the reel-in, a fraction of the energy is used to rewind the cable while the kite comes back.

In contrast to wind turbines, an AWES flight path is not unique. It can move freely within a prescribed flight envelope and its energy production is determined by its trajectory. Determining an optimal trajectory constitutes a complex optimization problem and vast study field [4, 5, 6].

Once an optimal trajectory is found, one still needs to fly it, requiring an ad hoc control system. The efficiency of the controller and its ability to follow the given reference trajectory directly impacts the system performance. The task is even more challenging when considering atmospheric flows, including turbulence, and eventually wakes from other devices. Haas et al. [7] were the first to consider this problem, a Large-Eddy Simulation (LES) framework was developed to study AWES farms in realistic turbulent winds. The AWES were represented by their main wing, modeled as an actuator sector. The system dynamics were computed using a 3-DOF (degrees of freedom) point-mass model coupled to a closed-loop path-tracking controller from the optimal control toolbox `AWEbox` [5]. In the study, a large mismatch was found between the aerodynamic forces computed with the actuator sector model in the LES framework and the force predictions of the 3-DOF point-mass model in `AWEbox`. Consequently, the Nonlinear Model Predictive Controller (NMPC) was not able to compensate this mismatch. Therefore, the LES-based forces could not be directly fed into the AWES dynamics. Instead, only the apparent wind evaluated by the LES framework was provided to the 3-DOF point-mass model, hence still capturing the main effects of turbulent wind fluctuations. Furthermore, the 3-DOF model only included the translational dynamics of the AWES, hence requiring additional assumptions to approximate the attitude and angular rates of the wing.

In the present work, our aim is to develop an LES framework using more accurate models of AWES in realistic turbulent winds. The trajectory generation and tracking is performed by `AWEbox`, using a 6-DOF aircraft model. The reference rigid-wing AWES from [4] is considered and is modeled using an actuator line (AL) for the wing. The effect of the control surfaces (elevator, rudders and ailerons) is also added, using models based on their geometry and lift slope, to allow for the computation of the aerodynamic moments; as required by the 6-DOF model. The AL-based model is coupled to the NMPC of `AWEbox` and is flown with closed-loop control. The model is then used to assess the controller robustness against turbulence, and to compare the performance between idealized conditions in `AWEbox` and turbulent wind conditions in the LES.

This study primarily focuses on an optimal one-loop optimal trajectory flown using flight path tracking within an LES simulation. Various quantities such as the states and controls applied to the aircraft are analyzed and compared to the reference, as computed using `AWEbox`. Additionally, the variations due to the turbulence intensity are also discussed. As a second investigation, we also show the case of a 4-loop trajectory. Section 2 details the methodology used in this work. The results are presented in Section 3 and the last section provides the conclusion and some perspectives for future research.

2. Methodology

2.1. Flow solver

The Large-Eddy Simulations are performed using a fourth-order finite difference solver for incompressible flows, developed at UCLouvain [8, 9]. Validation against direct numerical simulations (DNS) is reported in [8]. For LES, the subgrid-scale model employed is a regularized variational multiscale (RVM) model [10, 11]. The domain is discretized using a Cartesian staggered grid and the temporal integration is handled using a second-order Adams-Bashforth scheme. Synthetic turbulence is added to the inflow at the inlet in the form of Mann boxes [12].

2.2. Aircraft model

Within the flow solver, the main wing is modeled using an actuator line (AL) model [13]. This technique involves three main steps: first, the effective flow velocity is interpolated from the grid to the control points along the actuator line. Second, the aerodynamic forces are calculated based on the interpolated velocities and the airfoil polar data. Finally, these forces are distributed on

the flow solver grid. They are incorporated through the addition of a volumetric force term to the right hand side of the flow equations.
As Caprace et al. [14] showed, 2D regularization kernels (for both the velocity evaluation at the control points and the force distribution) better predict the aerodynamic forces than when using a 3D kernel. The regularization of the AL is therefore performed using a 2D Gaussian kernel; it is applied using in a planar template grid perpendicular to the line at the control point, and with pre-computed weights [15]. Linear interpolation is used to transfer velocity information from the flow grid to the template, and to transfer force information from the template to the flow grid.
The AWES considered here is the rigid-wing reference AWES called MegAWES [4]. It has a wing span of 42.5 m and an aspect ratio of 12. A sketch is shown in Figure 1a. Its planform section is the $\mathrm{RevE_{HC}}$ aerodynamic profile [16]; the two rudders and the elevator use a NACA0012 profile. Due to their small aspect ratio, those control surfaces cannot be adequately modeled using an AL; they are also too small compared to the affordable grid resolution of the flow solver to allow for a fine enough discretization. Their effect is hence taken into account using

$$L_{CS} = \frac{1}{2}\,\rho\,V^2\,A\frac{dC_L}{d\alpha}\,\alpha_{CS} \tag{1}$$

where A is the control surface area and $dC_L/d\alpha$ is its effective lift slope. It was evaluated using a lifting surface method; the result was found to be similar to that obtained using the Helmbold formula for low aspect ratios wings. The velocity V is interpolated from the flow solver grid at the location of the aerodynamic center of the control surface. This is done using a $M'4$ interpolation scheme [17]. From that information, the velocity magnitude and its angle of incidence with respect to the control surface are determined.

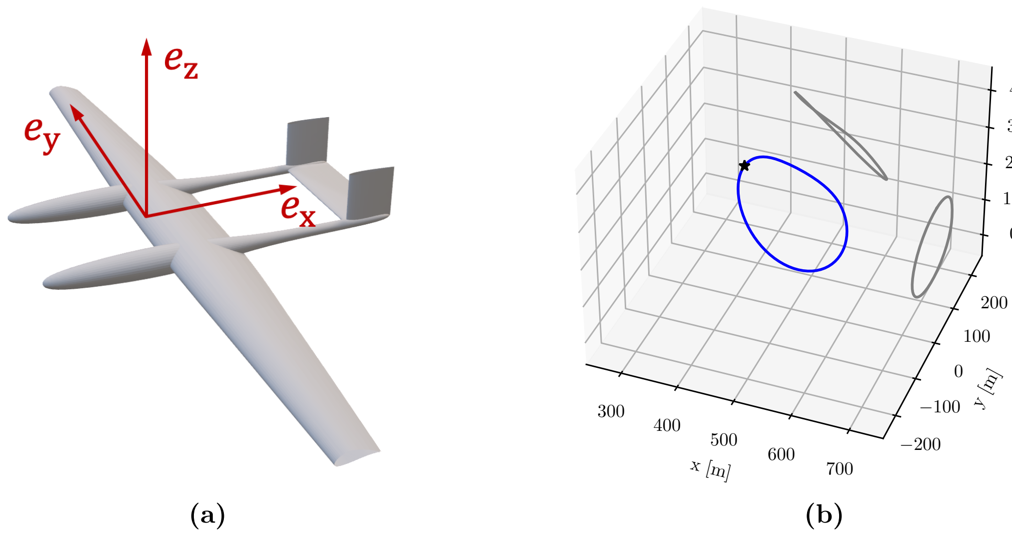

Figure 1: Representation of the MegAWES aircraft with the `AWEbox` body frame (a) and the one-loop optimal trajectory generated using `AWEbox` (b).

The effect of the ailerons is taken into account by modifying the local airfoil aerodynamic properties used in the AL, according to the aileron deflection. The lift per unit span on a wing section of chord c and concerned by an aileron deflection angle δ_a is

$$l(\alpha) = \frac{1}{2}\,\rho\,V^2\,c\,\left(C_l(\alpha) + \tau\,\frac{dC_l}{d\alpha}\,\delta_a\right) \tag{2}$$

where τ is an effectiveness factor [18], here obtained as 0.6. It accounts for the fact that the aileron does not span the whole chord and has a limited efficiency. The flow velocity is interpolated from that already obtained at the nearest control points of the AL. The forces acting on the control surfaces are small compared to the forces acting on the main wing and they are not added to the flow.

2.3. Optimal trajectories and control

In this work, the AWES flies optimal trajectories generated using the AWE modelling and optimization toolbox `AWEbox` [5]. The toolbox `AWEbox` solves optimal control problems (OCP) for power-optimal flight path generation and flight path tracking using non-linear model predictive control (NMPC). Reference flight paths are first pre-computed for specific mean wind conditions and a given set of operation constraints, and later flown with the NMPC controller in the LES framework. The toolbox is coupled to the flow solver with a two-way coupling: the aerodynamic forces and moments, evaluated by the AL model combined with the control surface models, for the current states are sent from the LES flow solver to the toolbox. The NMPC controller then evaluates the control actions to take, given the course deviation from the reference path. Subsequently, the toolbox integrates the 6-DOF AWES dynamics and sends the updated states of the aircraft to the flow solver.

2.4. Numerical setup

The trajectory is thus generated using `AWEbox`. The constraints applied to the state and control variables of the OCP are provided in Tables 1 and 2, where $\boldsymbol{q}$ is the position, $\boldsymbol{\omega}$ is the angular velocity, $\boldsymbol{\delta}$ is the deflection angle of the different control surfaces, l is the tether length and T_T is the traction force on the tether. These constraints are used for flight path tracking and are tightened by a factor 0.8 for the flight path optimization, while the spatial footprint is only reduced by $b/2$, where b is the wing span. The NMPC aircraft aerodynamic model is based on stability derivatives coefficient [19]. The coefficients of the AL-based model have been evaluated and used in the controller model. The trajectory consists of a single loop and can be visualized in Figure 1b. It has a time period of 15.0 s and a 700 kW average power.

Table 1: Bound constraints applied to state variable $\mathbf{x}$ used in the optimal control problem. The maximal lateral extent of the flight path and the maximal tether length are respectively set to $y_{\max} = 145\,\mathrm{m}$ and $l_{\max} = 1000\,\mathrm{m}$ to limit the spatial footprint of the trajectories.

Quantity Units	q_x [m]	q_y [m]	q_z [m]	$\boldsymbol{\omega}$ [°/s]	$\boldsymbol{\delta}$ [°]	l [m]	$\dot{l}$ [m/s]
Min.	0.0	$-(y_{\max}+0.5b)$	$2b$	−50.0	−20.0	0.0	−30.0
Max.	l_{max}	$+(y_{\max}-0.5b)$	$+\infty$	+50.0	+20.0	l_{max}	+30.0

The AWES flies a trajectory of diameter $D \simeq 5\,b = 212.5\,\mathrm{m}$. A mean wind velocity U_∞=10 m/s with added synthetic turbulence is imposed at the inlet and drives the flow in the computational domain. The size of the computational domain is $9\,D \times 3\,D \times 3\,D$, and the frontal area swept by the trajectory is less than 8% of the frontal area of the computational domain. The number of grid points is $768 \times 256 \times 256$ grid points. This results in about 17 grid points per wing span. We use periodic and slip boundary conditions in the transverse and vertical directions, respectively. An outflow boundary condition is used at the end of the domain. Turbulence is injected into the domain through $12\,D$-long Mann boxes, with various turbulence intensities, using the Kaimal

Table 2: Bound constraints applied to control variable $\mathbf{u}$ and other variables used in the optimal control problem. The maximum tether tension depends $T_{T,\max} = 1.7\,\text{MN}$ [4].

Quantity	$\dot{\boldsymbol{\delta}}$	$\ddot{l}$	T_T	$\ddot{\boldsymbol{q}}$
Units	[°/s]	[m/s^2]	[kN]	[g]
Min.	−50.0	−10.0	0.0	−3.0
Max.	+50.0	+10.0	$T_{T,\max}$	+3.0

spectrum. We start gathering the different aerodynamic and flow quantities after the flow and the wake have developed for one Mann box flow through time $T_{\text{mann}} = 12\,t^*$ where $t^* = \frac{U\,t}{D}$ and sample the data for one additional flow through time, up to $2T_{\text{mann}} = 24\,t^*$.

3. Results

The one-loop trajectory was flown for various levels of inflow turbulence intensity. The AWES positions are presented in the inertial frame (with x in wind direction and z upward) and the forces are presented in the AWES body frame, as used in `AWEbox`, see Figure 1. They are compared to the trajectory as optimized by `AWEbox`. We begin by discussing the results obtained under uniform inflow conditions and with high turbulence intensity. Subsequently, we focus on the results dependency to turbulence levels. We then conclude with some results obtained for a 4-loop trajectory.

3.1. Flight path tracking in uniform and turbulent inflows

The tracking of position and attitude over 17 loops is very accurate, as evidenced in Figure 2, with near perfect alignment to the target. Even for a turbulence intensity of 10%, the match remains strong with a mean difference compared to `AWEbox` within 2.5% for the position and within 5% for the attitude, as detailed in the next section. A shaded area indicating one standard deviation is also included. Its faint visibility confirms the controller's efficacy in compensating the course variations induced by the turbulence.

Concerning the control surface deflections displayed in Figure 3, the elevator actuation (δ_e) closely follows the reference while some deviations occur for the ailerons (δ_a) and rudders (δ_r): they experience the most significant variations as they are used to compensate the moment mismatch, as shown below, and the turbulence induced variations. The rudder is the most critical control surface due to its frequent deflection at maximum allowed angles for both optimization and tracking.

The cycle-averaged aerodynamic forces and moments evaluated by the AL-model are plotted in Figure 4 and compared to the `AWEbox` reference. Notably, the forces in thr x- and z-directions align well, while the force in the y-direction deviates more due to its dependence on the rudders, which do not precisely follow the target. The pitching moment about the y-axis matches closely that of the reference; more differences are observed for the two others. Again, those are mainly influenced by the control actions and their sensitivity to turbulence is thus also more important. Despite the observed differences, the mismatch of aerodynamic forces and moments is small enough to overcomes the coupling limitations observed by Haas et al. [7].

The match is also very good for the tether speed and the traction force, as seen in Figure 5. Their dependency to the turbulence level is low, and so is that of the power. The mean cycle power measured for the uniform inflow and 10% TI case is respectively 779 kW and 786kW. The difference between both cases being less than 1%, the system performances are therefore

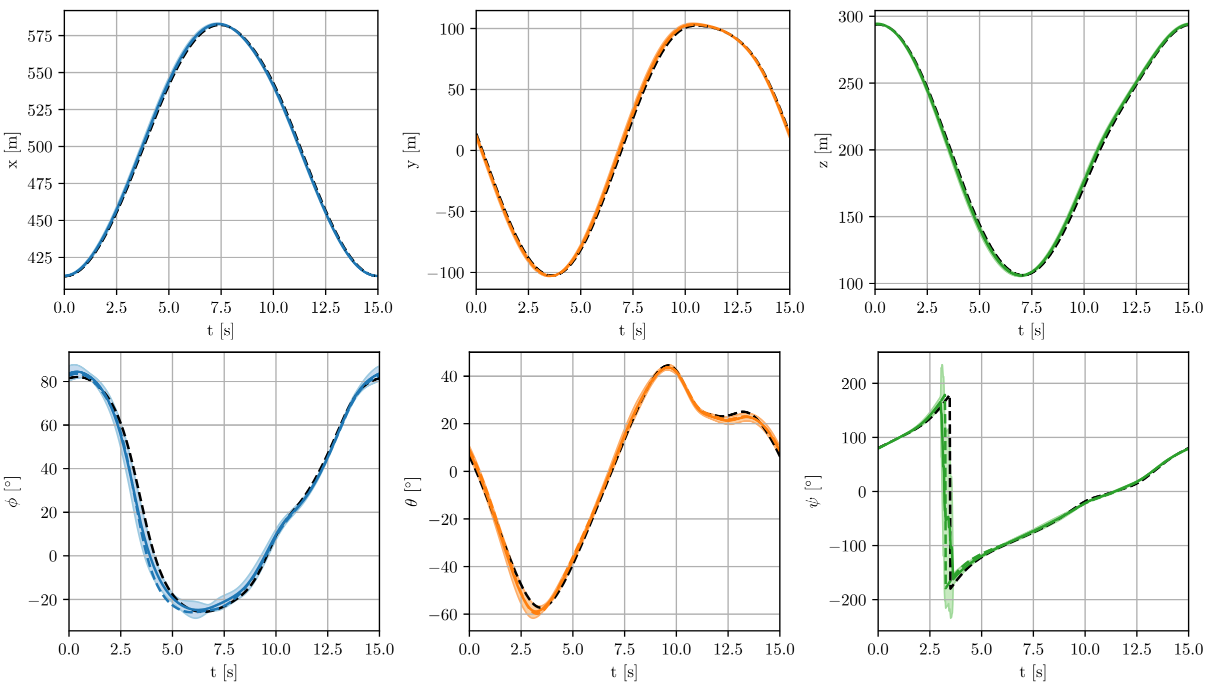

Figure 2: 17-cycle averaged position and Euler angles with their standard deviation (shaded area) for LES with AL: uniform (- -) and turbulent with 10% TI (—); `AWEbox` prediction (- -).

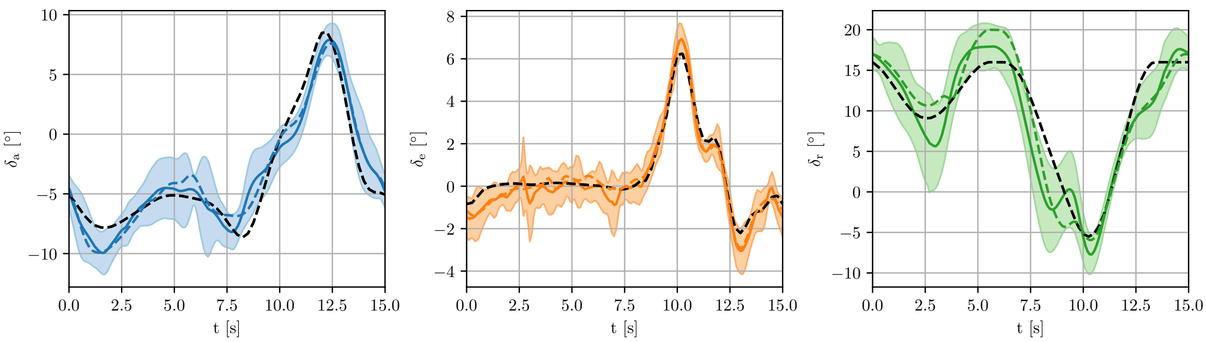

Figure 3: 17-cycle averaged actuation of the control surfaces with their standard deviation (shaded area) for LES with AL: uniform (- -) and turbulent with 10% TI (—); `AWEbox` prediction (- -).

only weakly sensitive to turbulence. Overall, the NMPC has proven reliable to track, in different turbulence conditions, the states and other aerodynamic quantities predicted by `AWEbox` for the given reference trajectory. In particular, the controller was able to accurately compensate the deviations from the flight path due to the aerodynamic force and moment fluctuations induced by turbulence.

3.2. Global quantification of differences for various turbulence intensities

When turbulence is introduced at the inflow, the mean cycle evaluated for the different quantities remains close to that under uniform inflow, as seen in Figures 2 to 4. Despite some differences noted with the `AWEbox` results, the main effects are the added fluctuations around the mean cycle. The mean cycles of the intermediate levels of turbulence experience a smooth transition

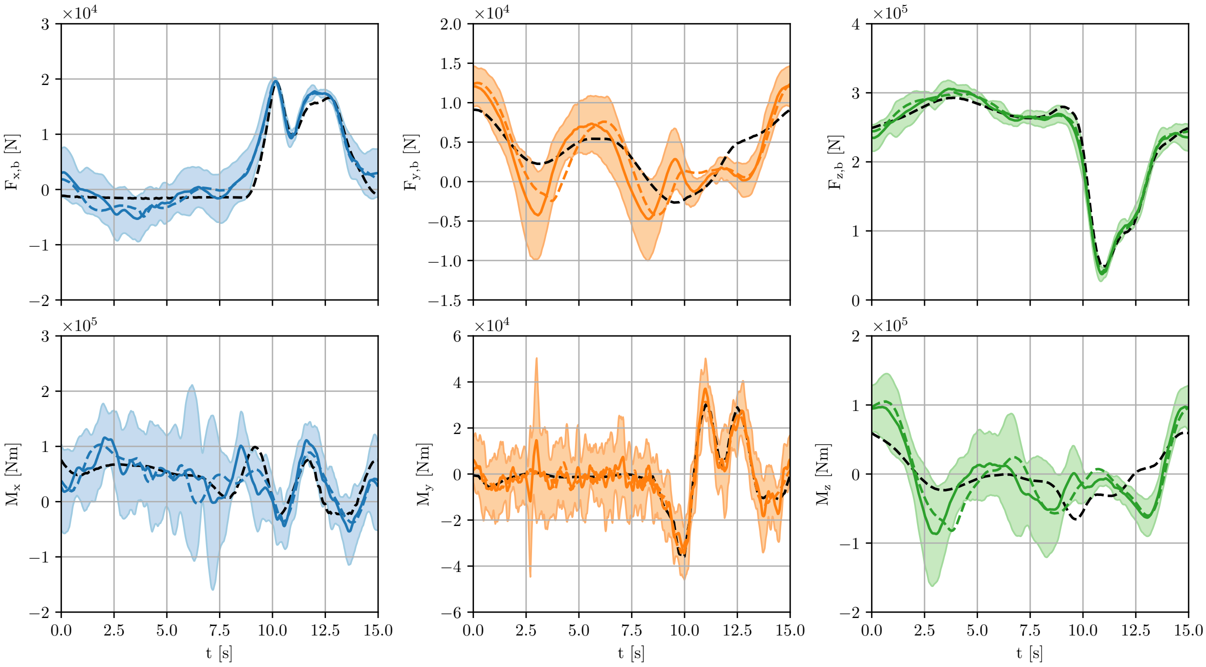

Figure 4: 17-cycle averaged forces in the `AWEbox` body frame and moments with their standard deviation (shaded area) using LES with AL: uniform (- -) and turbulent with 10% TI (—); `AWEbox` (- -).

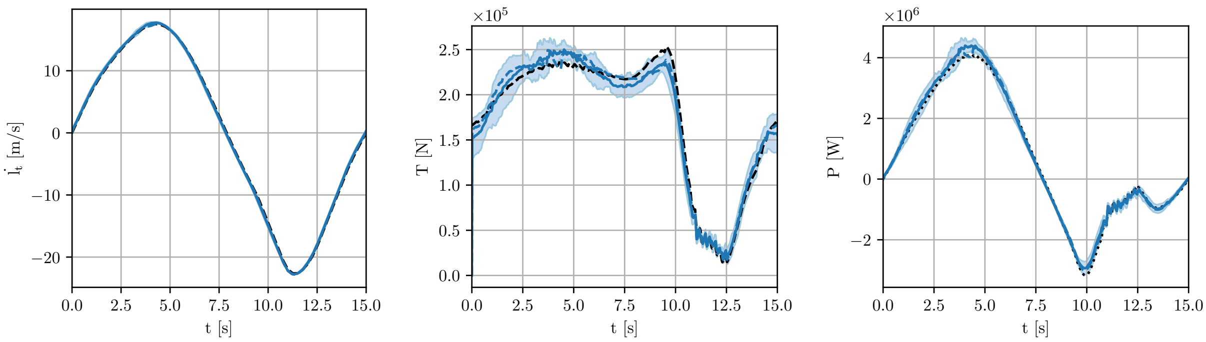

Figure 5: 17-cycle averaged tether speed, traction and power production with their standard deviation (shaded area) for LES with AL: uniform (- -) and turbulent with 10% TI (—); `AWEbox` (- -).

between the uniform and the high level 10% TI case. Figure 6 shows two different quantifications of the difference between a measured quantity and its mean cycle value or the `AWEbox` result. First, ϵ is the RMS difference relatively to the `AWEbox` result. We use the time-averaged $\overline{\epsilon(x_i,t)}/\max(x_i)$ to quantify globally the ability to track the target. Second, the time-averaged standard deviation $\overline{\sigma(x_i,t)}/\max(x_i)$ is used to quantify globally the variability added by the turbulence relatively to the mean cycle value. The position and attitude differences do not increase much with turbulence and the variations that may be induced remains very small. The NMPC is very good at closely tracking the reference for those two quantities. For the control surface deflection, the difference is mainly on the ailerons and rudders. It grows with the turbulence intensity. This reflects the action of the controller to compensate the forces

Journal of Physics: Conference Series **2767** (2024) 072021 doi:10.1088/1742-6596/2767/7/072021

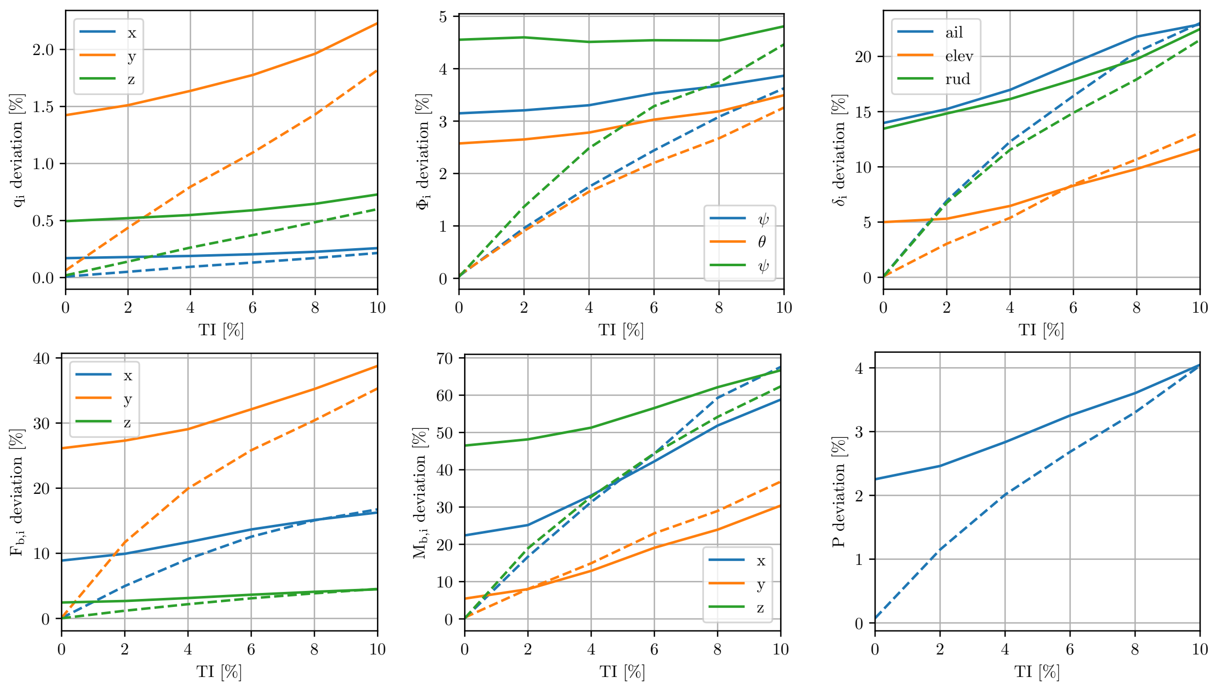

Figure 6: 17-cycle averaged deviation. RMS difference relatively to the reference $\overline{\epsilon(x_i,t)}/\max(x_i)$ (—) and standard deviation relatively to the obtained mean value $\overline{\sigma(x_i,t)}/\max(x_i)$ (- -).

fluctuations. The force in the y-direction shows the largest error and dependency to turbulence as it is closely linked to the rudder. The force in the z-direction shows the lowest error and sensitivity to turbulence, helping to make the power error and sensitivity low as well. The reference power is, along with the position and velocity, very well followed. The moments show the largest error and sensitivity to turbulence. Nevertheless, the deviations due to the fluctuations of the aerodynamic forces and moments are well enough compensated by the NMPC. The controller response for the different turbulence levels, observed through the controls $\dot{\boldsymbol{\delta}}$ and $\ddot{l}_t$, stays within the specified bounds without being saturated. Despite the fact that turbulence induces some deviation from the reference, along with time variations, no remarkable observations were identified. For the control surfaces deflection rates, $\overline{\epsilon(x_i,t)}/\max(x_i)$ and $\overline{\sigma(x_i,t)}/\max(x_i)$ both almost reach 100% for the highest level of turbulence. They stay below 10% for the tether acceleration.

3.3. Four-loop trajectory

Finally, we also investigate the controller ability to fly a 4-loop trajectory. It has a time period of 60.0 s and a 715 kW average power. The ascending phase of the last loop is used for the reel-in. It is flown in a turbulence with 6% TI. As for the 1-loop trajectory, the controller is able to accurately track its target path and the power produced is also very close to the reference, as shown in Figure 7. Note that `AWEbox` has no generator model. Accounting for the drum could lead to different results for the trajectory. For example, it could try to limit the number of negative tether speed (and thus negative power) periods during one cycle. In the considered trajectory, it pulls on the tether at each ascending phase to help the kite going up.

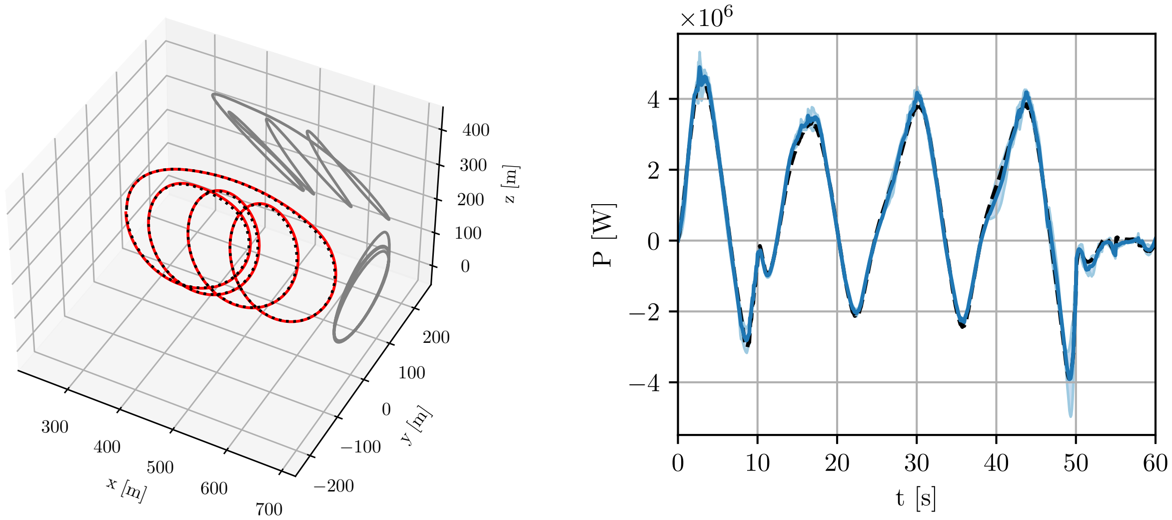

Figure 7: Trajectory and power for a 4-loop trajectory flown in turbulence with 6% TI. The power obtained for LES with AL is plotted with its standard deviation (shaded area) (—); `AWEbox` prediction (- -).

4. Conclusion and perspectives

In this work, an in-house LES framework using an actuator line (AL) method to model the main wing is further developed and coupled with the NMPC controller of `AWEbox`. The use of the 6-DOF model required to add aerodynamic models to take into account the effect of the control surfaces. The results show that the use of the 6-DOF model allows the controller to accurately track the reference trajectory despite the forces and moments mismatch and the large fluctuations due to the inflow turbulence. Therefore, the implementation of the 6-DOF AWES model with active control surfaces and its coupling with our LES-AL framework overcomes the modelling and coupling limitations first observed by Haas et al. [7]. It is shown that, even with high turbulence level, the controller is still able to track very well the target path despite the forces and moments variations. The impact of the turbulence was found to mainly add variations around the average behaviour, while the error does not grow significantly. The system performances have not been found to be significantly affected by the turbulence level. Then, the controller also showed its ability to follow a 4-loop trajectory.

An improvement to this work will further investigate the trajectory generation and the choice of the values for the different bounds and constraints applied to the OCP variables (it might then not be necessary to restrict all the variables by 0.8, as done so far). A sensitivity study shall be conducted. The study already demonstrates the successful coupling of the LES-AL framework with the NMPC controller of `AWEbox` and it shows that this control strategy can reliably steer the AWES despite high levels of wind turbulence. This important milestone further facilitates the investigation of more complex scenarios. Firstly, more realistic inflow conditions could be considered, such as an atmospheric boundary layer with shear instead of a uniform inflow with synthetic turbulence. Secondly, the behavior of the kite when it is subjected to perturbations such as gusts or varying wind conditions (direction or intensity) could be investigated. Finally, the impact of another device wake, such as from wind turbines or other AWES, could be studied. This will typically happen when an AWES will be located close to another device or wind farm, or when they are themselves arranged in arrays or wind farm. Studying such scenarios would allow to gain insight in the controller's ability to manage such events but also to quantify how this affects the energy production, or the loads felt by the wing to ensure the structural integrity of the future real devices.

5. Acknowledgements

This work is carried out as part of the BORNE project on “Developing the tools and insight to expand the Belgian offshore wind farms with airborne wind energy systems”, funded by the Energy Transition Funds from the SPF Economy. The present research benefited from computational resources made available on Lucia, the Tier-1 supercomputer of the Walloon Region, infrastructure funded by the Walloon Region under the grant agreement n°1910247. We also thank Jochem De Schutter for his assistance with the toolbox AWEbox.

6. References

[1] Loyd M L 1980 Journal of Energy **4** 106–111
[2] van Hagen L, Petrick K, Wilhelm S and Schmehl R 2023 Energies **16**
[3] Cherubini A, Papini A, Vertechy R and Fontana M 2015 Renewable and Sustainable Energy Reviews **51** 1461–1476
[4] Eijkelhof D and Schmehl R 2022 Renewable Energy **196** 137–150
[5] De Schutter J, Leuthold R, Bronnenmeyer T, Malz E, Gros S and Diehl M 2023 Energies **16**
[6] Vermillion C, Cobb M, Fagiano L, Leuthold R, Diehl M, Smith R S, Wood T A, Rapp S, Schmehl R, Olinger D and Demetriou M 2021 Annual Reviews in Control **52** 330–357
[7] Haas T, De Schutter J, Diehl M and Meyers J 2022 Wind Energy Science **7** 1093–1135
[8] Duponcheel M, Bricteux L, Manconi M, Winckelmans G and Bartosiewicz Y 2014 International Journal of Heat and Mass Transfer **75** 470–482
[9] Moens M, Duponcheel M, Winckelmans G and Chatelain P 2018 Wind Energy **21** 766–782
[10] Jeanmart H and Winckelmans G 2007 Physics of Fluids **19** 055110
[11] Cocle R, Bricteux L and Winckelmans G 2009 Physics of Fluids **21** 085101
[12] Mann J 1994 Journal of Fluid Mechanics **273** 141–168
[13] Sørensen J N and Shen W Z 2002 Journal of Fluids Engineering **124** 393–399
[14] Caprace D G, Winckelmans G and Chatelain P 2020 Theoretical and Computational Fluid Dynamics **34** 21–48
[15] Trigaux F, Chatelain P and Winckelmans G 2022 Journal of Physics: Conference Series **2265** 022050
[16] Eijkelhof D 2019 Delft University of Technology & Technical University of Denmark
[17] Monaghan J J 1985 Journal of Computational Physics **60** 253–262
[18] McCormick B 1995 Aerodynamics, Aeronautics, and Flight Mechanics (Wiley)
[19] Malz E, Koenemann J, Sieberling S and Gros S 2019 Renewable Energy **140** 1004–1011